JACS
JOURNAL OF THE AMERICAN CHEMICAL SOCIETY
Communication
pubs.acs.org/JACS

$Sb@Ni_{12}@Sb_{20}^{-/+}$ and $Sb@Pd_{12}@Sb_{20}^{n}$ Cluster Anions, Where n = +1, −1, −3, −4: Multi-Oxidation-State Clusters of Interpenetrating Platonic Solids

Yi Wang,[†] Melanie Moses-DeBusk,[†] Lauren Stevens,[†] Junkai Hu,[†] Peter Zavalij,[†] Kit Bowen,[‡] Brett I. Dunlap,[#] Evan R. Glaser,[#] and Bryan Eichhorn*[,†]

[†]Department of Chemistry and Biochemistry, University of Maryland, College Park, Maryland 20742, United States
[‡]Departments of Chemistry and Materials Science, Johns Hopkins University, Baltimore, Maryland 21218, United States
[#]U.S. Naval Research Laboratory, Codes 6189 and 6877, Washington, D.C. 20375-5347, United States

Supporting Information

ABSTRACT: K_5Sb_4 and K_3Sb_7 Zintl ion precursors react with $Pd(PPh_3)_4$ in ethylenediamine/toluene/PBu_4^+ solutions to give crystals of $Sb@Pd_{12}@Sb_{20}^{n-}/PBu_4^+$ salts, where n = 3, 4. The clusters are structurally identical in the two charge states, with nearly perfect I_h point symmetry, and can be viewed as an $Sb@Pd_{12}$ icosahedron centered inside of an Sb_{20} dodecahedron. The metric parameters suggest very weak Sb−Sb and Pd−Pd interactions with strong radial Sb−Pd bonds between the Sb_{20} and Pd_{12} shells. All-electron DFT analysis shows the 3− ion to be diamagnetic with I_h symmetry and a 1.33 eV HOMO−LUMO gap, whereas the 4− ion undergoes a Jahn−Teller distortion to an S = 1/2 D_{3d} structure with a small 0.1 eV gap. The distortion is predicted to be small and is not discernible by crystallography. Laser desorption−ionization time-of-flight mass spectrometry (LDI-TOF MS) studies of the crystalline samples show intense parent $Sb@Pd_{12}@Sb_{20}^-$ ions (negative ion mode) and $Sb@Pd_{12}@Sb_{20}^+$ (positive ion mode) along with series of $Sb@Pd_{12-y}@Sb_{20-x}^{-/+}$ ions. Ni(cyclooctadiene)$_2$ reacts with K_3Sb_7 in en/tol/Bu_4PBr solvent mixtures to give black precipitates of $Sb@Ni_{12}@Sb_{20}^{n-}$ salts that give similar $Sb@Ni_{12}@Sb_{20}^{-/+}$ parent ions and $Sb@Ni_{12-y}@Sb_{20-x}^{-/+}$ degradation series in the respective LDI-TOF MS studies. The solid-state and gas-phase studies of the icosahedral $Sb@M_{12}@Sb_{20}^{n-/n+}$ ions show that the clusters can exist in the −4, −3, −1, +1 (M = Pd) and +1, −1 (M = Ni) oxidation states. These multiple-charge-state clusters are reminiscent of redox-active fullerenes (e.g., C_{60}^n, where n = +1, 0, −1, −2, −3, −4, −5, −6).

Icosahedral metal clusters with I_h molecular symmetry have large orbital degeneracies and often possess special properties and stabilities. For example, gas-phase endohedrally centered icosahedral clusters, such as Al_{13}^- (i.e., $Al@Al_{12}^-$) and related compounds,[1,2] exhibit greater stability than their non-icosahedral compositional neighbors, such as Al_{12}^- and Al_{14}^-. Their icosahedral assemblies result in unusual reactivities attributed to their unique jellium-like electronic structures.[2,3] The fullerene C_{60} also has I_h molecular symmetry and highly degenerate HOMO (five-fold-degenerate H_u symmetry) and LUMO (three-fold-degenerate T_{1u} symmetry) orbital configurations with a 1.5 eV HOMO−LUMO gap.[4] This electronic structure also gives rise to special properties, such as the remarkable electrochemical behavior involving six reversible reductions and one quasi-reversible oxidation.[5−7] The three-fold degeneracy of the parent LUMO in C_{60} allows for the six sequential one-electron reductions that occur at relatively consistent 450 ± 50 mV intervals. As a result, C_{60} has eight accessible oxidation states that can be generated in solution. While multi-oxidation-state coordination complexes are known, such as the M(bipyridine)$_3$ complexes,[8,9] the redox activity is primarily ligand based, and electron correlation is limited. The redox behavior of C_{60} and its fullerene relatives is unique[7] and tied to the orbital degeneracies associated with their high-symmetry structures.

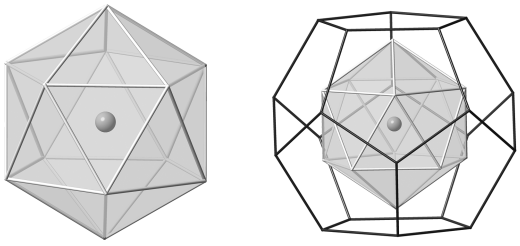

Figure 1. Schematic drawings of the $M@E_{12}^{n-}$ (left) and $E@M_{12}@E_{20}^{n-}$ (right) clusters, where M is a transition metal and E is a main group element.

In contrast to gas-phase chemistry, icosahedral transition metal clusters in the condensed phase are rare. Main-group centered Ni_{12} carbonyl complexes, such as $E@Ni_{12}(CO)_{22}^{2-}$, where E = Sn, Ge, have icosahedral geometry but are distorted from I_h point symmetry.[10] More recently, a number of icosahedral main group clusters have been prepared from Zintl ion precursors, such as the diamagnetic $M@Pb_{12}^{n-}$ (M = Ni, Pd, Pt, n = 2; M = Rh, Ir, n = 3)[11−14] and $M@Sn_{12}^{3-}$ ions (M = Rh, Ir).[13,15] These ligand-free icosahedral clusters (Figure 1) have rigorous I_h point symmetry, formally d^{10} endohedral metal atoms, and highly degenerate electronic states.[11] Attempts to oxidize or reduce these clusters have met with limited success. For example, $Pt@Pb_{12}^{n-}$ retains its icosahedral structure in both the −1 and −2 oxidation states,[16]

Received: November 23, 2016
Published: December 24, 2016

DOI: 10.1021/jacs.6b12109
J. Am. Chem. Soc. 2017, 139, 619−622

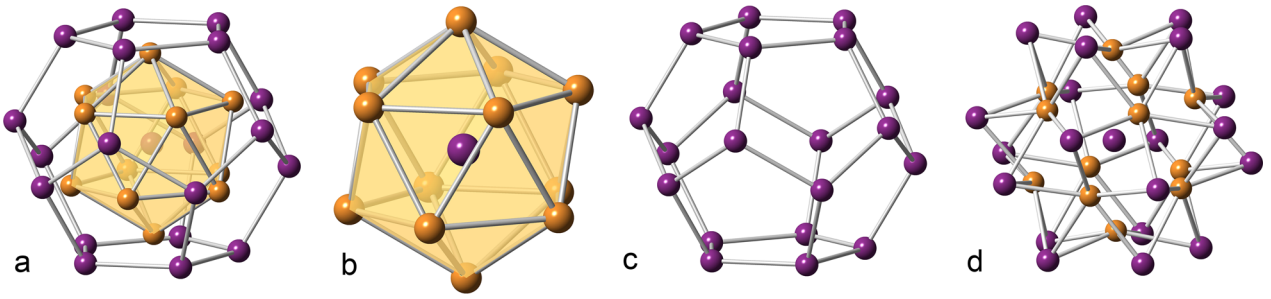

Figure 2. X-ray crystal structure of $Sb@Pd_{12}@Sb_{20}^{4-}$ ion (Sb is violet, Pd is gold) showing (a) the 33-atom structure represented as interpenetrating dodecahedral Sb_{20} and icosahedral $Sb@Pd_{12}$ shells. Pd−Sb bonding is omitted for clarity. (b) The $Sb@Pd_{12}$ icosahedron. (c) The Sb_{20} dodecahedron. (d) An identical view of the full 33-atom cluster showing only the Pd−Sb bonds between the Sb_{20} and Pd_{12} shells. Bonds to the endohedral Sb and the weak Pd−Pd and Sb−Sb interactions are omitted for clarity.

but further reductions or oxidations have not been successful to date. Attempts to lower the electron counts in the $M@E_{12}$ cluster system by employing earlier transition metals with fewer electrons result in lower symmetry non-icosahedral structures such as $Ru@Ge_{12}^{3-}$ and $V@Ge_8As_4^{3-}$ clusters with 3-connected cage vertices.[17,18]

Another intriguing icosahedral structure involves the nested "onion-skin" clusters of formula $E@M_{12}@E_{20}^{n-}$ (Figure 1), where M is a metal atom and E is a main group element.[19] These clusters can be viewed as an $E@M_{12}$ icosahedron centered inside of an E_{20} dodecahedron. Because both Platonic solid substructures have I_h point symmetry, the interpenetrating $E@M_{12}@E_{20}^{n-}$ structures also possess this symmetry. While this general cluster type is known in some solid-state compounds (i.e., clathrates and $Mg_{32}(Al,Zn)_{49}$-type intermetallics),[20] there are only two reported examples of this structure as an isolated unit. The $A_{12}Cu_{12}Sn_{21}$ ternary phases (A = K, Na)[21] contain isolated $Sn@Cu_{12}@Sn_{20}^{12-}$ cluster subunits separated by alkali cations. The only molecular example of this structure type is the $As@Ni_{12}@As_{20}^{3-}$ ion[22] prepared from a solution reaction between the As_7^{3-} Zintl ion and $Ni(COD)_2$, where COD = cyclooctadiene. Both clusters have nearly ideal I_h point symmetry with large electronic degeneracies.

We describe here two new series of $Sb@M_{12}@Sb_{20}^{n}$ clusters where M = Pd and Ni. Through gas-phase mass spectrometry and single-crystal X-ray diffraction studies (XRD), we have identified charge states for the Pd cluster, where n = 4−, 3−, 1−, and 1+. While the $Sb@Pd_{12}@Sb_{20}^{3-}$ is a diamagnetic complex with nearly perfect I_h point symmetry, DFT studies show the paramagnetic $Sb@Pd_{12}@Sb_{20}^{4-}$ cluster to be Jahn−Teller distorted with a D_{3d} ground-state structure and a small 0.1 eV band gap. The predicted distortion from the I_h structure is small and is not discernible in the single-crystal structure of the ion. These studies suggest that a general class of I_h $E@M_{12}@E_{20}$ complexes can exist in various oxidation states, which is directly analogous to the fullerenes.

The reaction between K_5Sb_4 and $Pd(PPh_3)_4$ in ethylenediamine (en)/toluene (tol) solvent mixtures containing Bu_4PBr gives dark brown plates of $[Bu_4P]_4[Sb@Pd_{12}Sb_{20}]\cdot 4tol$ in ca. 5% yield based on Pd. The salt contains the $Sb@M_{12}@Sb_{20}^{4-}$ ion (Figure 2) and is described below. The cluster is paramagnetic with an $S = 1/2$ ground state (see below). Electron paramagnetic resonance (EPR) spectra of the crystalline solid reveals a g-value of 2.0036 and full width at half maximum (fwhm) of 9.6 G (Figure S7). A similar reaction between K_3Sb_7 and $Pd(PPh_3)_4$ in en/tol/Bu_4PBr solvent mixtures results in the formation of black needle-like crystals of $[Bu_4P]_3[Sb@Pd_{12}Sb_{20}]\cdot 3.5en$ in ca. 15% yield based on Pd. This salt contains the $Sb@Pd_{12}@Sb_{20}^{3-}$ ion (Figure S1), which is structurally indistinguishable from $Sb@Pd_{12}@Sb_{20}^{4-}$ (Figure 2). Small amounts (ca. 2%) of the $[Bu_4P]_4[Sb@Pd_{12}Sb_{20}]\cdot 4tol$ crystals also form in this reaction, suggesting that the −3 and −4 charge states of the cluster coexist in solution. Both salts have been characterized by single crystal XRD, energy dispersive X-ray analysis (EDX), and laser desorption/ionization time-of-flight mass spectrometry (LDI-TOF MS). Similar reaction between $Ni(COD)_2$ and K_3Sb_7 in en/tol/Bu_4PBr solvent mixtures gives black precipitates of $Sb@Ni_{12}@Sb_{20}^{n-}$ salts that have been clearly identified through LDI-TOF MS studies. While the cluster is most likely in the $Sb@Ni_{12}@Sb_{20}^{3-}$ charge state in the condensed phase, we have not isolated crystalline samples of this material and have only identified the $Sb@Ni_{12}@Sb_{20}^{-/+}$ ions in the gas phase (see below).

The structures of the $Sb@Pd_{12}@Sb_{20}^{n-}$ clusters (n = 3 or 4) are virtually identical and only differ by the types of solvates and the number of cations in the respective crystal lattices. A summary of the metric parameters and comparisons with the $As@Ni_{12}@As_{20}^{3-}$ and $Sn@Cu_{12}@Sn_{20}^{12-}$ ions are given in Table 1 and S1.

Table 1. Average Bond Distances (Å) for $E@M_{12}@E_{20}^{n-}$ Clusters (E = As, Sb, Sn; M = Pd, Ni, Cu)[a]

	E−M_{12}	M−M	E−E	M_{12}−E_{20}
$As@Ni_{12}@As_{20}^{3-}$ [22]	2.557 (2)	2.689(4)	2.752(3)	2.395(5)
$Sb@Pd_{12}@Sb_{20}^{3-}$	2.856(20)	3.003(10)	3.109(34)	2.713(45)
$Sb@Pd_{12}@Sb_{20}^{4-}$	2.8538(3)	3.0009(5)	3.1063(5)	2.7114(6)
$Sn@Cu_{12}@Sn_{20}^{12-}(Na)$ [21]	2.631(5)	2.766(12)	3.104(5)	2.766(9)
$Sn@Cu_{12}@Sn_{20}^{12-}(K)$ [21]	2.625(3)	2.759(8)	3.097(5)	2.760(7)

[a]The E−M_{12} bonds are to the central μ_{12} atom. The M_{12}−E_{20} bonds are to the outer E_{20} shell.

Summaries of the crystallographic data are given in Tables S2 and S3. The $[Bu_4P]_3[Sb@Pd_{12}Sb_{20}]\cdot 3.5en$ salt is monoclinic, space group $P2_1/n$, with the $Sb@Pd_{12}Sb_{20}^{3-}$ ion centered on a general position. The $[Bu_4P]_4[Sb@Pd_{12}Sb_{20}]\cdot 4tol$ salt is also monoclinic, but possesses $C2/m$ crystal symmetry. In this structure, the center of the $Sb@Pd_{12}Sb_{20}^{4-}$ ion resides on the 2c Wykoff position with crystallographically imposed 2/m symmetry. One PBu_4^+ counterion was disordered in each of the structures.

The 33-atom structures can be viewed as interpenetrating cluster subunits defined by $Sb@Pd_{12}^{n-}$ icosahedra nested inside of Sb_{20} dodecahedra (Figure 2b,c). The charges on the complexes are clearly distributed across the entire clusters (see below), but from an 8-N Zintl-type analysis, one can view all of the three-connected Sb atoms in the Sb_{20} cages as neutral. This analysis is

DOI: 10.1021/jacs.6b12109
J. Am. Chem. Soc. 2017, 139, 619−622

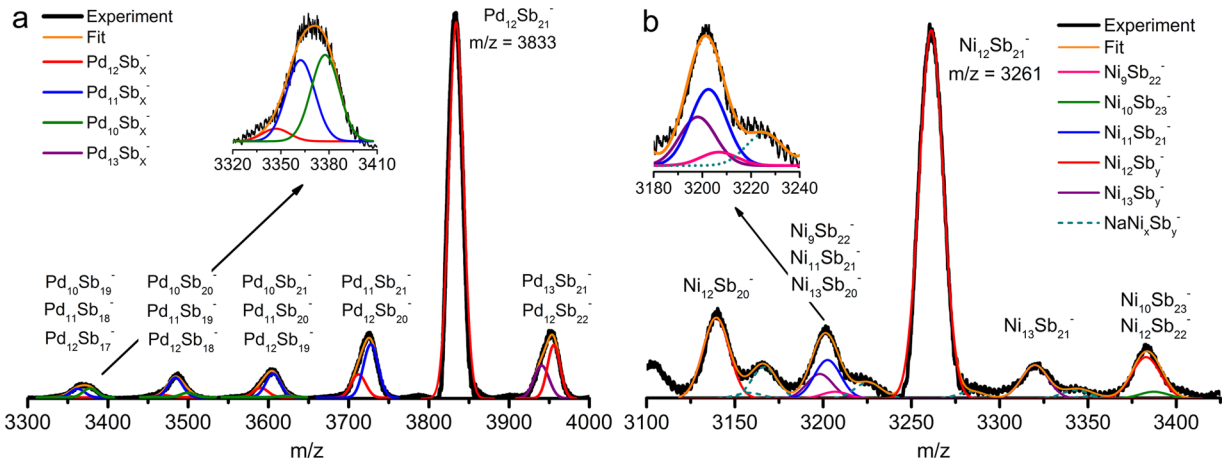

Figure 3. (a) LDI-TOF mass spectrum of $Sb@Pd_{12}@Sb_{20}^{3-}$ (negative ion mode) showing the molecular ion at $m/z = 3833$ and the $Pd_{12}Sb_{21-x}^-$ ($x = 1-10$) and $Pd_{12-y}Sb_{21-x}^-$ ($y = 1-3$) cluster series. The overlapping mass envelopes were deconvoluted as shown in the insets and the cluster ion populations are given in Figure S2. (b) LDI-TOF mass spectrum of $Sb@Ni_{12}@Sb_{20}^{n-}$ (negative ion mode) showing the $Ni_{12}Sb_{21-x}^-$ ($x = 1-10$) and $Ni_{12-y}Sb_{21-x}^-$ ($y = 1-3$) series. The sodium ion impurity peaks are labeled (green dashed line).

akin to $As@Ni_{12}@As_{20}^{3-}$ and simplifies as Sb^{3-}, Pd_{12}^0, and Sb_{20}^0 for the diamagnetic $Sb@Pd_{12}Sb_{20}^{3-}$ ion complex. The extra electron in the $Sb@Pd_{12}Sb_{20}^{4-}$ ion resides in a nominally degenerate H_g state (before Jahn–Teller distortion, see below), similar to C_{60}.

The central $Sb@Pd_{12}$ icosahedron in each anion is virtually identical with Pd–Pd and Sb–Pd bond distances of 3.00(1) Å and 2.86(1) Å, av., respectively. The Pd–Pd distances are 9.5% longer than those in Pd metal (2.74 Å) and related organometallic Pd–Sb clusters (2.96 Å, av.),[23,24] which is only slightly more than the 7.6% elongation of the Ni–Ni contacts of $As@Ni_{12}@As_{20}^{3-}$ relative to Ni metal (2.50 Å).[25] In contrast, the Pd–Sb contacts to the centered Sb are similar to Pd–Sb contacts in organostibnide Pd clusters (2.69 Å, av.)[23,24,26,27] and Pd–Sb intermetallics (2.75 Å, av.).[28,29] In all of the $E@M_{12}@E_{20}^{n-}$ structures (Table S3), the $E-M_{12}/M-M$ ratio is 0.951, which is equal to the ideal geometric value.[30]

The Sb–Sb contacts average 3.11 Å in the Sb_{20} dodecahedral shells of both clusters and are quite long for typical 2-center 2-electon (2c-2e) bonds. For comparison, Sb–Sb contacts in $R_2Sb-SbR_2$ organostibnides are typically 2.83–2.87 Å in length[31,32] and Sb–Sb contacts in polystibnide Zintl clusters are typically in the range 2.81–2.98 Å.[33,34] While the 3-connected Sb environments in the Sb_{20} cages are suggestive of traditional 2c-2e bonding with an Sb lone pair, the Sb–Sb bond distances are indicative of weak fractional or secondary bonding interactions.[35] In contrast, the Pd–Sb contacts to the Sb_{20} cages ($M_{12}-E_{20}$, 2.71 Å, av.) seem to be more robust and typical of Pd–Sb interactions in related intermetallics and clusters.

Strong radial $M_{12}-E_{20}$ bonding with weaker M–M and E–E bonding seems to be characteristic of this cluster type in that analogous trends are observed in the $Sn@Cu_{12}@Sn_{20}^{12-}$ and $As@Ni_{12}@As_{20}^{3-}$ clusters (Table 1).[21,22,36] While it may be convenient to highlight the Platonic-like dodecahedral and icosahedral subshells when deconstructing the overall cluster (Figure 2b,c), it is more accurate to represent the structure in terms of the strong $M_{12}-E_{20}$ bonds while omitting the weaker M–M and E–E bonds (Figure 2d). Various bonding models have been used to describe the electronic structures of related clusters, such as jellium cluster analysis, cluster valence analysis and Wade–Mingos analysis.[19,21,22] Below, we describe the structure and bonding in terms of all-electron DFT analysis.

All-electron calculations were performed on the $Sb@Pd_{12}@Sb_{20}^{3-/4-}$ clusters using the DGauss DZVP double-ζ orbital basis with matching A2 auxiliary basis set.[37] The analytic density-functional method[38] with exchange-correlation parameter 0.7 was used to compute electronic structures. The $Sb@Pd_{12}@Sb_{20}^{3-}$ molecular geometry was optimized in icosahedral symmetry with a net molecular charge of −3. The cluster is diamagnetic with 228 total valence electrons. The highest occupied molecular orbital is 36 t_{1u}, the lowest unoccupied molecular orbital is 45 h_g, and the gap is 1.33 eV. The calculated bond distances and angles are in excellent agreement with the experimental data (Table S1). The same methods applied to $As@Ni_{12}@As_{20}^{3-}$ yield the same frontier-orbital irreducible representations and a slightly larger HOMO–LUMO gap of 1.58 eV.

The $Sb@Pd_{12}@Sb_{20}^{4-}$ cluster has a single unpaired electron in the h_g orbital set. In this state, the g_g and h_g geometrical distortions then become Jahn–Teller active.[39] The g_g distortion leads to minimal energy lowering in a D_{2h} state. The h_g distortion leads to a lower-energy D_{3d} state containing a small 0.1 eV gap, which appears to be the ground state. The optimized D_{3d} structure is virtually indistinguishable from the idealized I_h structure as evidenced by the calculated bond distances given in the Table S1. The distortion is not resolved in the single-crystal structure, which is not surprising in view of the spherical nature of the cluster. In isolation, the unpaired h_g electron is unbound and the calculated fourth electron affinity is less than −5 eV. These results have been confirmed by equivalent Gaussian09 calculations.

LDI-TOF MS data were collected from single crystals of the $[Bu_4P]_3[Sb@Pd_{12}Sb_{20}]\cdot 3.5en$ salt suspended on carbon tape. The data (Figure 3a) show a strong parent ion peak at $m/z = 3833$ with a mass envelope characteristic of the expected statistical distribution of ^{121}Sb (57%) and ^{123}Sb (43%) isotopes and the six naturally occurring Pd isotopes in the 33-atom cluster. In addition, a series of $Pd_{12}Sb_{21-x}^-$ (x = 1–10) and $Pd_{12-y}Sb_{21-x}^-$ ($y = 1-3$) cluster anions are formed in the laser ablation process and seem to be characteristic of this class of compounds (e.g., $As@Ni_{12}@As_{20}^{3-}$).[22] The $Pd_{12-y}Sb_{21-x}^-$ ($y = 1-3$) series appears as a low-mass tail on the primary $Pd_{12}Sb_{21-x}^-$ peaks. The population evolution of the high-mass peaks is shown in the spectral deconvolutions of the mass envelopes (Figures 3a and S2). There are also overlapping peaks for $Pd_{13}Sb_{21}^-$ and $Pd_{12}Sb_{22}^-$ due to the

DOI: 10.1021/jacs.6b12109
J. Am. Chem. Soc. 2017, 139, 619–622

attachment of an additional Pd atom and Sb atom, respectively, to the parent cluster. Analysis of the same sample in the positive ion mode shows the $Pd_{12}Sb_{21}^{+}$ ion in the gas phase, along with other $Pd_{12-y}Sb_{21-x}^{+}$ clusters (Figure S3). As with virtually all Zintl-type clusters in the gas phase, only singly charged ions are detected by mass spectrometry. In all cases, the molecular ion is the most intense peak in the high-mass region of the spectrum.

LDI-TOF MS data for the Ni−Sb reactions (Figure 3b) show the presence of $Sb@Ni_{12}@Sb_{20}^{-}$ as evidenced by the characteristic parent ion at $m/z = 3261$ and the corresponding $Ni_{12}Sb_{21-x}^{-}$ and $Ni_{12-y}Sb_{21}^{-}$ series of clusters. In contrast to the $Sb@Pd_{12}@Sb_{20}^{3-}$ cluster, the $Sb@Ni_{12}@Sb_{20}^{n-}$ complex shows a far more prominent set of $Ni_{12-y}Sb_{21}^{-}$ cluster anions due to Ni loss in laser ablation process. The Ni−Sb sample also contains Na^{+} ion-paired clusters (i.e., $NaNi_{12}Sb_{20}^{-}$) resulting from Na^{+} impurities, however, ion pairing with the molecular ion was not clearly evident in these studies or LDI-TOF studies with K^{+}-doped $Sb@Pd_{12}@Sb_{20}^{3-}$ crystals.

The solid-state and gas-phase studies of the icosahedral $Sb@E_{12}@Sb_{20}^{n-/n+}$ ions show that the clusters can exist in the −4, −3, −1, and +1 oxidation states (M = Pd). We have not yet detected clusters in the −2 or neutral charge states, which could have appeared in the form of $KPd_{12}Sb_{21}^{-}$ (i.e., the K^{+} $Pd_{12}Sb_{21}^{2-}$ ion pair) or $KPd_{12}Sb_{21}^{+}$ (i.e., the K^{+} $Pd_{12}Sb_{21}^{0}$ ion pair). While there is some evidence of these clusters in the $NaNi_{12}Sb_{21}$ series (Figure S4), definitive proof is still missing. Regardless, these observations suggest that multiple oxidation states of the clusters might be accessible in solutions, representing a new class of multi-oxidation-state high-symmetry clusters.

■ ASSOCIATED CONTENT

Supporting Information

The Supporting Information is available free of charge on the ACS Publications website at DOI: 10.1021/jacs.6b12109.

Experimental details, and supporting Figures S1−S9, and Tables S1−S4 (PDF)
X-ray data for $[Bu_4P]_3[Sb@Pd_{12}@Sb_{20}]\cdot 3.5en$ (CIF)
X-ray data for $[Bu_4P]_4[Sb@Pd_{12}@Sb_{20}]\cdot 4tol$ (CIF)

■ AUTHOR INFORMATION

Corresponding Author

*eichhorn@umd.edu

ORCID

Yi Wang: 0000-0001-9866-2376
Melanie Moses-DeBusk: 0000-0003-0382-0824

Notes

The authors declare no competing financial interest.

■ ACKNOWLEDGMENTS

We thank the Office of Naval Research (MURI-Cliff Bedford program manager, grant N00014-15-1-2681) for support of this work. B.I.D. and E.R.G thank the Office of Naval Research and Naval Research Laboratory for financial support.

■ REFERENCES

(1) Bergeron, D. E.; Castleman, A. W.; Morisato, T.; Khanna, S. N. *Science* **2004**, *304*, 84.
(2) Burgert, R.; Schnöckel, H.; Olzmann, M.; Bowen, K. H. *Angew. Chem., Int. Ed.* **2006**, *45*, 1476.
(3) Burgert, R.; Stokes, S. T.; Bowen, K. H.; Schnöckel, H. *J. Am. Chem. Soc.* **2006**, *128*, 7904.
(4) Östling, D.; Rosén, A. *Chem. Phys. Lett.* **1993**, *202*, 389.
(5) Xie, Q.; Arias, F.; Echegoyen, L. *J. Am. Chem. Soc.* **1993**, *115*, 9818.
(6) Echegoyen, L.; Echegoyen, L. E. *Organic Electrochemistry*, 4th ed.; Lund, H., Hammerich, O., Ed.; CRC Press: New York, 2001; p 323.
(7) Echegoyen, L.; Echegoyen, L. E. *Acc. Chem. Res.* **1998**, *31*, 593.
(8) Scarborough, C. C.; Wieghardt, K. *Inorg. Chem.* **2011**, *50*, 9773.
(9) DeCarlo, S.; Mayo, D. H.; Tomlinson, W.; Hu, J.; Hooper, J.; Zavalij, P.; Bowen, K.; Schnöckel, H.; Eichhorn, B. *Inorg. Chem.* **2016**, *55*, 4344.
(10) Ceriotti, A.; Demartin, F.; Heaton, B. T.; Ingallina, P.; Longoni, G.; Manassero, M.; Marchionna, M.; Masciocchi, N. *J. Chem. Soc., Chem. Commun.* **1989**, 786.
(11) Esenturk, E. N.; Fettinger, J.; Lam, Y. F.; Eichhorn, B. *Angew. Chem., Int. Ed.* **2004**, *43*, 2132.
(12) Esenturk, E. N.; Fettinger, J.; Eichhorn, B. *J. Am. Chem. Soc.* **2006**, *128*, 9178.
(13) Downing, D. O. Ph.D. Dissertation, University of Maryland, College Park, MD, 2012.
(14) Wang, Y.; Wang, L.-L.; Ruan, H.-P.; Luo, B.-L.; SANG, R.-L.; Xu, L. *Chin. J. Struct. Chem.* **2015**, *34*, 1253.
(15) Wang, J. Q.; Stegmaier, S.; Wahl, B.; Fässler, T. F. *Chem. - Eur. J.* **2010**, *16*, 1793.
(16) Grubisic, A.; Wang, H.; Li, X.; Ko, Y.-J.; Kocak, F. S.; Pederson, M. R.; Bowen, K. H.; Eichhorn, B. W. *Proc. Natl. Acad. Sci. U. S. A.* **2011**, *108*, 14757.
(17) Espinoza-Quintero, G.; Duckworth, J. C.; Myers, W. K.; McGrady, J. E.; Goicoechea, J. M. *J. Am. Chem. Soc.* **2014**, *136*, 1210.
(18) Mitzinger, S.; Broeckaert, L.; Massa, W.; Weigend, F.; Dehnen, S. *Chem. Commun.* **2015**, *51*, 3866.
(19) Huang, X.; Zhao, J.; Su, Y.; Chen, Z.; King, R. B. *Sci. Rep.* **2014**, *4*, 6915.
(20) Bergman, G.; Waugh, J. L.; Pauling, L. *Acta Crystallogr.* **1957**, *10*, 254.
(21) Stegmaier, S.; Fässler, T. F. *J. Am. Chem. Soc.* **2011**, *133*, 19758.
(22) Moses, M. J.; Fettinger, J. C.; Eichhorn, B. W. *Science* **2003**, *300*, 778.
(23) Fenske, D.; Persau, C. *Z. Anorg. Allg. Chem.* **1991**, *593*, 61.
(24) Benjamin, S. L.; Krämer, T.; Levason, W.; Light, M. E.; Macgregor, S. A.; Reid, G. *J. Am. Chem. Soc.* **2016**, *138*, 6964.
(25) Wells, A. F. *Structural inorganic chemistry*; 5th reprint ed.; Oxford University Press: Oxford, 2012.
(26) Stark, J. L.; Harms, B.; Guzman-Jimenez, I.; Whitmire, K. H.; Gautier, R.; Halet, J.-F.; Saillard, J.-Y. *J. Am. Chem. Soc.* **1999**, *121*, 4409.
(27) Adams, R. D.; Pearl, W. C., Jr; Wong, Y. O.; Zhang, Q.; Hall, M. B.; Walensky, J. R. *J. Am. Chem. Soc.* **2011**, *133*, 12994.
(28) Brese, N. E.; von Schnering, H. G. *Z. Anorg. Allg. Chem.* **1994**, *620*, 393.
(29) (a) Okada, A.; Kobayashi, K.; Ito, T.; Sakurai, T. *Acta Crystallogr., Sect. C: Cryst. Struct. Commun.* **1991**, *47*, 1358. (b) Marsh, R. *Acta Crystallogr., Sect. A: Found. Crystallogr.* **1994**, *50*, 450.
(30) Fässler, T. F.; Hoffmann, S. D. *Angew. Chem., Int. Ed.* **2004**, *43*, 6242.
(31) Westerhausen, M.; Weinrich, S.; Mayer, P. *Z. Anorg. Allg. Chem.* **2003**, *629*, 1153.
(32) Breunig, H.; Rösler, R. *Coord. Chem. Rev.* **1997**, *163*, 33.
(33) Critchlow, S. C.; Corbett, J. D. *Inorg. Chem.* **1984**, *23*, 770.
(34) Bolle, U.; Tremel, W. *J. Chem. Soc., Chem. Commun.* **1992**, 91.
(35) Alcock, N.-W. *Adv. Inorg. Chem. Radiochem.* **1972**, *15*, 1.
(36) King, R. B.; Zhao, J. *Chem. Commun.* **2006**, 4204.
(37) Godbout, N.; Salahub, D. R.; Andzelm, J.; Wimmer, E. *Can. J. Chem.* **1992**, *70*, 560.
(38) Dunlap, B. I. *J. Phys. Chem. A* **2003**, *107*, 10082.
(39) Jahn, H. A.; Teller, E. *Proc. R. Soc. London, Ser. A* **1937**, *161*, 220.

DOI: 10.1021/jacs.6b12109
J. Am. Chem. Soc. 2017, 139, 619−622